Laboratory Study of the Crystallization of Sodium Chloride from Brine

Anthony Scrutton

Research and Development, Winnington Laboratory, Imperial Chemical Industries, Ltd., (Mond Division), Northwich, Cheshire CW8 4DJ, England

ABSTRACT

The evaporative crystallization of sodium chloride from purified ammonia-soda brine has been studied using a laboratory continuous mixed suspension mixed product removal crystallizer (CMSMPR), with a crystal production rate of 1 kg/hr. The crystallizer design incorporated a pneumatic product removal system which allowed the crystal residence time, magma concentration and production rate to be varied independently.

When producing cubic habit crystals, growth rates were found to be independent of crystal size for crystals larger than 75 μm, that is McCabe's ΔL law was obeyed. This law was not obeyed when the product contained a large proportion of partly spherical or spherical crystals.

The crystal growth and nucleation rates observed at constant magma concentration, over a range of residence times and stirrer speeds fit a Power law model of the type $B^0 = k_R M G^g N^j$ in which k_R varied with stirrer design.

INTRODUCTION

ICI operates a very large number of processes involving crystallization. In tonnage terms, one of the main ones is the evaporative crystallization of sodium chloride from brine. Production evaporators vary widely in size and design, output ranges from a few to tens of tons per hour of salt. These evaporators have been, and still are, mainly designed from accumulated experience, because progress in understanding the basic mechanisms responsible for crystal growth and nucleation has been difficult and slow. Further, with this process, it is difficult to measure the prevailing supersaturation in an evaporator because it is so small. Some idea of the supersaturation levels to be expected can be deduced with the aid of Rumford and Bain's (1) data, and is found to be in the range σ, 6×10^{-3} to 1×10^{-5}.

Over the past ten years considerable advances have been made in the understanding of the crystallization unit process. This has been due to the development of the Randolph-Larson population balance theory and the use of the continuous mixed suspension mixed product removal (CMSMPR) laboratory crystallizer (2) to obtain the kinetic data. The advantage of this modern theory from a salt crystallization point of view is that the process can be characterized without the need to know the prevailing supersaturation. Since its development, the population balance approach has been tested on and applied to a wide variety of processes, particularly those of cooling and salting out. It has also been used to analyze the evaporative crystallization process theoretically, by Larson and Garside (3), the results obtained from a pilot size evaporator, by Bennett, Fiedelman and Randolph (4), and in a study on fines dissolution in the heat exchanger of a forced circulation evaporator, by Asselbergs and de Jong (5). However, the kinetics of evaporative crystallization of salt from brine have still not been elicited.

This paper describes the design of a laboratory evaporative crystallizer which closely approximates to the ideal CMSMPR, and some of the results obtained with it.

OUTLINE THEORY

The crystal growth and nucleation kinetics are most conveniently represented by the empirical equations.

Growth $$G = k_g S^n \quad (1)$$

Nucleation $$B^\circ = k_n M^j S^m \quad (2)$$

The most important kinetic consideration in design and analysis (particularly in the case of the salt-brine system as mentioned above) is the relationship between the nucleation and growth kinetics obtained by eliminating S from the above equations to give

$$B^\circ = k_R M^j G^i \quad (3)$$

where $i = m/n$ and $k_R = k_n/k_g^{m/n}$

A plot of $\log \frac{B^\circ}{M}$ vs log G will be a straight line of slope i, provided $j = 1$.

In a paper in 1970, Randolph (6) suggested that when plotting log B° vs log G there were three distinct regions, viz (Fig. 1): A) a metastable region of nucleation by attrition and seeding, B) secondary nucleation mechanisms operative only, and C) primary nucleation mechanisms operative. Power law kinetics given by equation 3 above describe secondary nucleation mechanisms in B. It can be inferred from a number of recent papers that in region B the value of the exponent i is low, i.e. 1 to 2, but is high in region C, i.e. 5 to 10.

The size distribution produced in an MSMPR crystallizer is given by

$$M = 6 f_v \rho n^\circ (G\tau)^4 \quad (4)$$

and the nucleation rate by $$B^\circ = G n^\circ \quad (5)$$

eliminating n° from the above equations, rearranging and taking logs, gives

$$\log \frac{B^\circ}{M} = \log\left(\frac{1}{6 f_v \rho \tau^4}\right) - 3 \log G \quad (6)$$

This expression relates nucleation rate with growth rate at constant solids (salt) residence time, and shows that as one increases the other decreases. A change in nucleation and growth rate results from a change in external factors, such as hydrodynamics (stirring), or impurities.

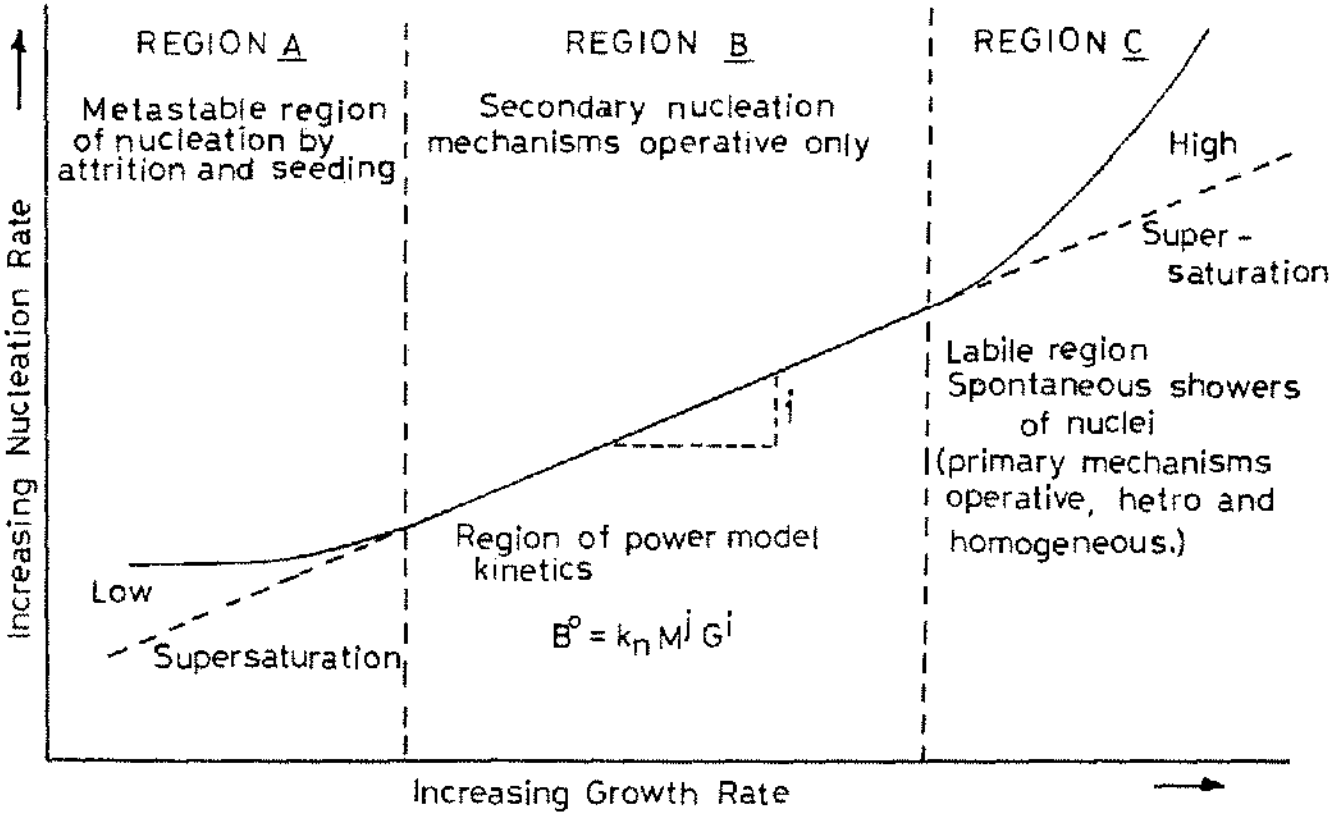

Figure 1. Regions of crystallization mechanisms.

EXPERIMENTAL

Design and construction of the crystallizer. The design of the crystallizer used for the work was that of a stirred vessel with a draft tube, similar to that used by Murray and Larson (7) and Mullin and Garside (8). The inside diameter is 20 cm and the overall height is 76 cm; with a liquor volume of 10.5 liters. A cut away diagram is shown in Figure 2. The cross-sectional area of the draft tube is half that of the vessel (equal area). There are four baffles in the vessel-draft tube annulus, three inside the latter above the stirrer to eliminate vortexing and four below to straighten out the magma flow. The circulation patterns with this configuration were visually checked with a glass and plastic model using crystals of different sizes, with different stirrer speeds. The stirrer is situated halfway up the draft tube, and the clearance between the propeller blade tips and the draft tube is 2 mm.

All parts of the crystallizer and ancillaries are designed to operate at atmospheric pressures and above, over the range of brine temperatures 109 to 165°C; and those in contact with hot brine made from Monel metal or cast iron.

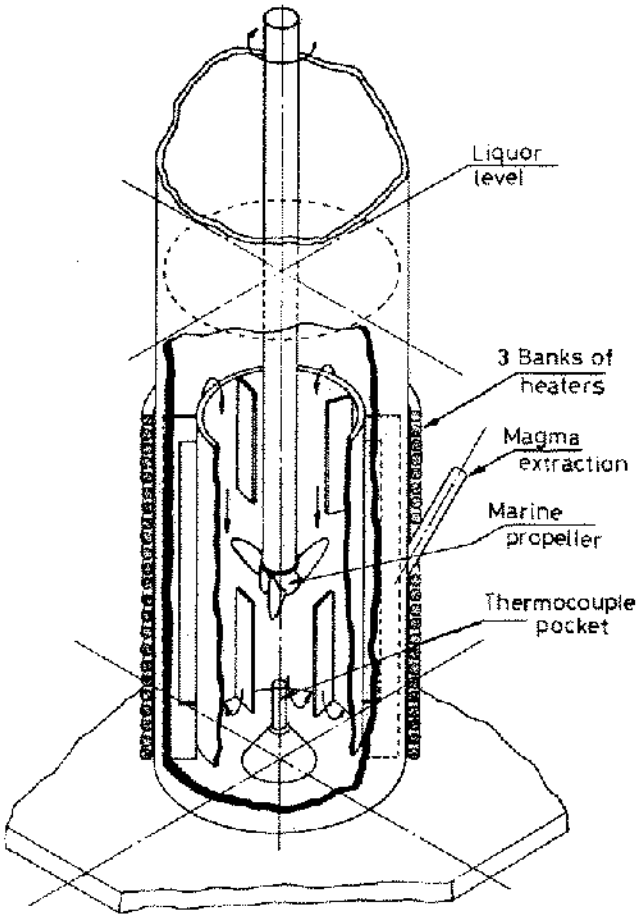

Figure 2. Evaporative crystallizer.

The heating for the crystallizer is provided by three Pyrobar electric elements, coiled around the outside lower one-third of the vessel body; one of 3 kW and two of 2 kW. The temperature of the brine in the crystallizer is controlled by the vapor pressure which is in turn controlled by a Glocon-Annin valve and Foxboro controller, normal fluctuations being $<\pm 1.4$°C. Vapor is condensed in a coiled tube stainless steel condenser.

Magma extraction system. With the most common designs of CMSMPR crystallizers, an aliquot of not more than 10% of the magma in the crystallizer is withdrawn intermittently either by a pump or by level control. For two reasons, neither of these systems was thought suitable; a) because of vapor 'flashing' and brine cooling problems, and b) it was required to conserve as much heat as possible to obtain a high salt production rate.

The system adopted is shown schematically in Figure 3.

An aliquot of magma is withdrawn intermittently from the crystallizer along a short pipe inclined at 30°, and tangentially into a separation vessel, by a pneumatic pump. The separation vessel contains an inner cylindrical compartment, which alternately empties and fills with 600 ml of brine. The salt crystals descend from the separation vessel by gravity into a 'salt box' or as required into a sample vessel. The clear brine is then returned to the crystallizer on the return stroke of the pneumatic pump.

The frequency of withdrawal of the magma aliquot (time T_1) and the time interval required to 'clarify the magma' (time T_2) is obtained by two Crouzet Timers. T_1 is determined by the preselected rate of salt production and required operating solids concentration. T_2 is preselected so that the probability of returning crystals of size >30 μm to the crystallizer is very small (assuming plug flow and free settling). Assuming a degree of non plug flow in the separation vessel, this gives an increasing probability of returning crystals of size <30 μm with decreasing crystal size.

The rate of magma withdrawal and brine return is fixed by restrictor on the pneumatic pump, and is preselected so that the fluid velocity up the exit pipe exceeds the fluid velocity in the vessel-draft tube annulus (approximately isokinetic withdrawal).

Crystallizer characteristics and operating conditions. The maximum salting and water evaporation rates are 1.2 and 3.2 kg/h respectively; this is obtained with a total power usage of 4.8 kW. The minimum salt crystal residence time achievable is 0.25 h, the maximum limited only by the need to operate shift working.

Two types of stirrer were used, a Marine propeller 0.137 m diameter and pitch 1.5; and an axial turbine—four blades at 45° 0.134 m diameter. The discharge coefficient k_p where $k_p = \frac{Q}{ND^3}$ for each stirrer was measured in brine at ambient temperature using a 'Novar Stream Flo' instru-

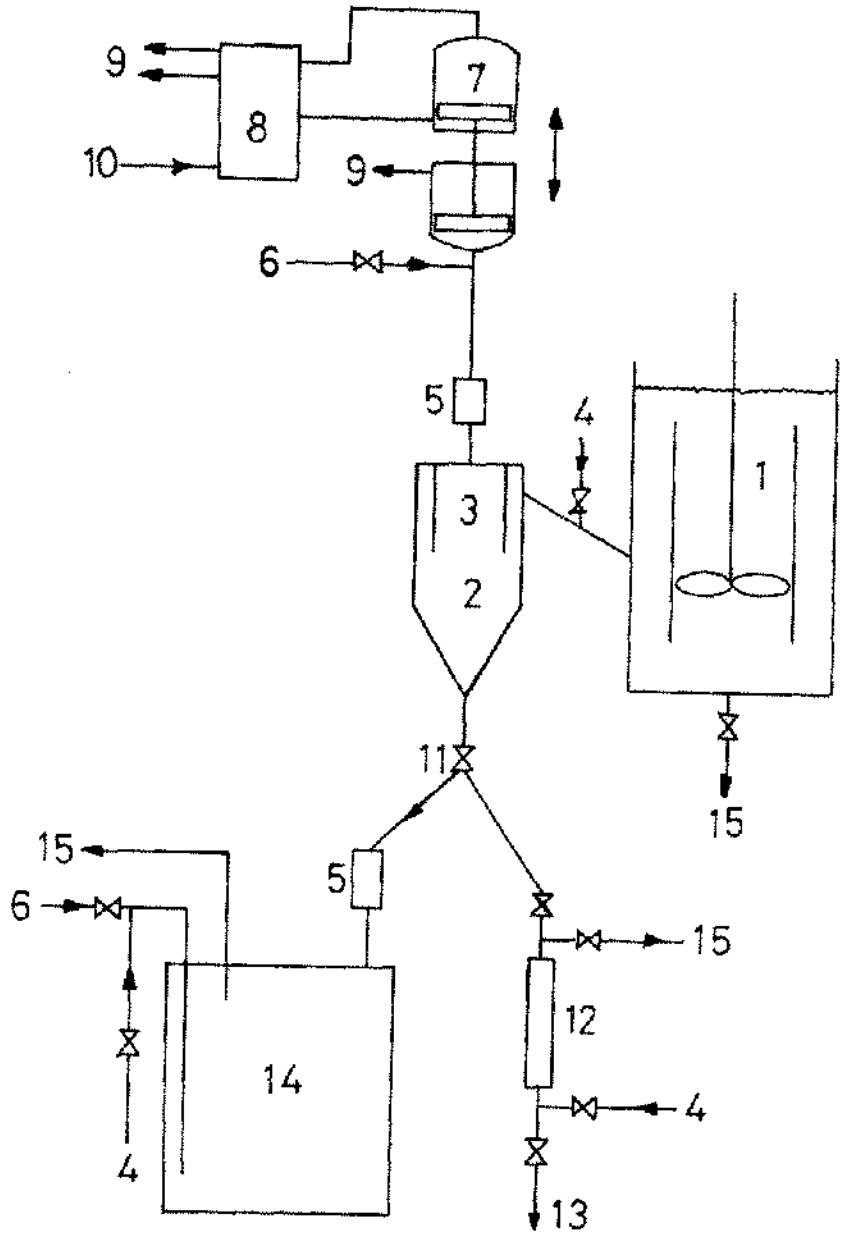

1 Evaporative crystalliser
2 Salt separation vessel
3 Air pocket
4 Brine entry
5 Sight glass
6 Water wash
7 Pneumatic cylinder
8 Pneumatic piston control valve
9 Air exhaust
10 Compressed air
11 Diversion valve
12 Sample vessel
13 Sample of salt
14 Salt box
15 Brine to drain

Figure 3. Magma extraction system (schematic).

ment and a neutral buoyancy follower. The values found were 0.35 and 0.39 respectively.

For all experimental work reported here, purified ammonia-soda brine was used, similar to that supplied to the production plants; the crystallizer was operated in the temperature range 109 to 115°C and within the magma concentration range 40 to 90 kg/m³. The length of the experimental runs was nine to fifteen salt crystal residence times.

At the end of each experimental run, two samples of approximately 60 g each, of the salt being produced were taken half an hour apart. From these the carrier brine was removed, and they were washed first with an ethanol-water mixture to remove residual brine and then with acetone. Finally, the samples were dried under an infra-red lamp, and sieve analysis carried out with Standard British sieves using a Pascall Inclino shaking machine.

The crystal growth and nucleation rates were obtained from the sieve analysis using the Population Density (2) and Cumulative Numbers (9) methods. In both cases, the line of best fit for the calculated values of the population density at a given mean size, or the cumulative numbers greater than a given size, was obtained. In addition, the values of n° and $G\tau$ (in the case of the population density) were used to calculate M using equation 4 and compared with its actual value. In most cases the former was within the range 98 to 105% of the latter; when this agreement was not achieved, the best values of n° and $G\tau$ that satisfied both criteria were accepted.

To confirm that the crystallizer was well mixed and classification was not occurring to a significant degree in the separation vessel, the solids concentration and crystal size distribution of product samples taken during several experimental runs and samples taken simultaneously from the body of the crystallizer were compared. No significant difference was observed.

RESULTS AND DISCUSSION

Effect of stirrer design on population density plots. Figure 4 shows a typical steady state population density obtained with the marine propeller stirrer, when producing cubic habit crystals. Similar straight line plots over the crystal size range 120 to 1200 μm were obtained with this stirrer at other speeds. These straight lines show that with these conditions, the growth rate is independent of crystal size, that is, that McCabe's ΔL law is obeyed.

Figure 5 shows a typical steady state population density obtained with the axial turbine stirrer. With this type the crystals produced were 'rounded' to varying degrees depending on its speed. It can be seen that the plot has a definite curvature, indicating that the system is not obeying the ΔL law. It is suggested that the reason for this is that mass is removed from the larger crystals which are trapped in the stirrer 'collision corridor' as suggested by C. Ramshaw (10), in varying amounts depending on size. It is to be expected that the energy and probability of impact of the larger crystals within this design of stirrer will be greater than with the marine propeller design.

Crystallization kinetics. To determine the value of the exponent i in equation 3, a series of measurements of growth and nucleation rates was carried out over a range of residence times from 0.4 to 1.5 h, with the marine propeller stirrer. First at 5.85 rev/s and then at 10.8 rev/s. The results obtained are shown in Figure 6 where B°/M is plotted vs G. Both sets of data can be correlated by straight lines of slope 2.0. To confirm that the value of the exponent is 2.0, a third series of measurements was carried out with the axial turbine stirrer at 10.8 rev/s, over a range of residence times from 0.29 to 1.27 h. The results obtained are shown in Figure 7. As with the previous sets of results, the data can be correlated by a straight line of slope 2.0. However, in this case there is a larger degree of scatter of the points about the line, due to the difficulty of obtaining the line of best fit to the population density data as shown in Figure 5.

The crystallization kinetics of the sodium chloride-water-ethanol salting out system has been studied by Koros et al. (11) and Yih-An Liu and Botsaris (12) in a CMSMPR crystallizer. The former workers found i to be 1.72, and the latter found it to be in the range 2.4 to 2.55. These are close to the value of 2.0 found herein.

During the establishment of the value of the exponent i, detailed analysis of the data partially established the relationship given by equation 6. This was confirmed by carrying out a series of measurements at a constant residence time of 0.625 h with both stirrers, at different speeds. The results of these are shown in Figure 8. The data points are correlated by a line of slope -3.0, and the intercept is 3.1×10^9 which is the expected value of $\frac{1}{6f_v\rho\tau^4}$.

Figure 9 shows the complete kinetic data obtained for the system over the range of operating conditions given herein. Also shown are the salt residence time data lines for 0.5, 1.0 and 1.5 h of slope -3.0. It can be seen that the kinetics are depicted by a 'grid' or 'carpet diagram'. With this diagram and using the MSMPR relationship $L_m = 3.67\ G\tau$, the product median size can be rapidly found for a given set of conditions.

In Figure 10 the variation of the parameter $\frac{B^\circ}{MG^2}$ with speed N for the two types of stirrer is shown. The data can be correlated by a line of slope 2.0. Thus for the marine propeller, the overall kinetics are given by the relationship

$$B^\circ = 0.120\ MG^2N^2 \qquad (7)$$

and for the Axial turbine

$$B^\circ = 0.191\ MG^2N^2 \qquad (8)$$

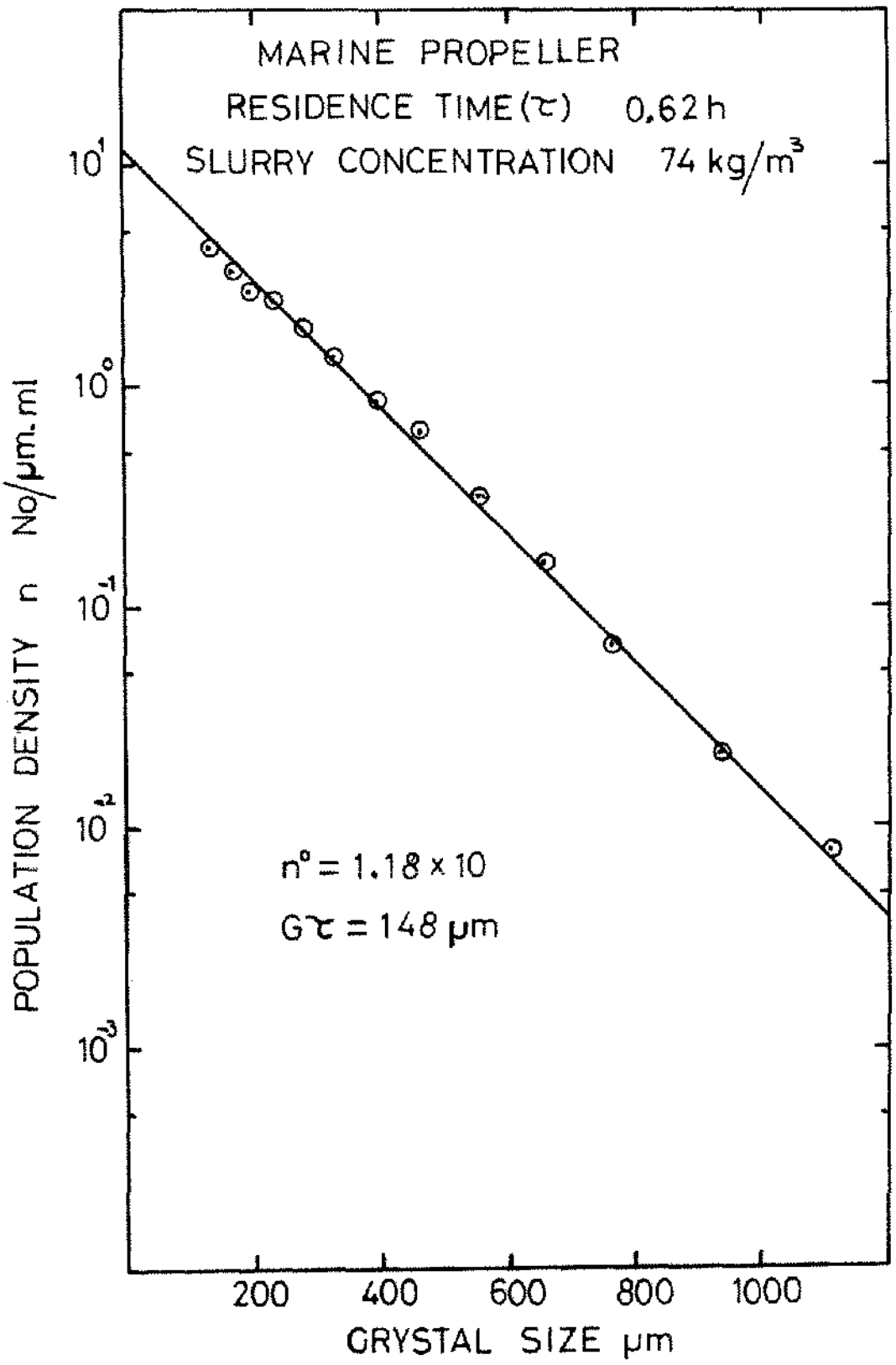

Figure 4. Steady-state population density.

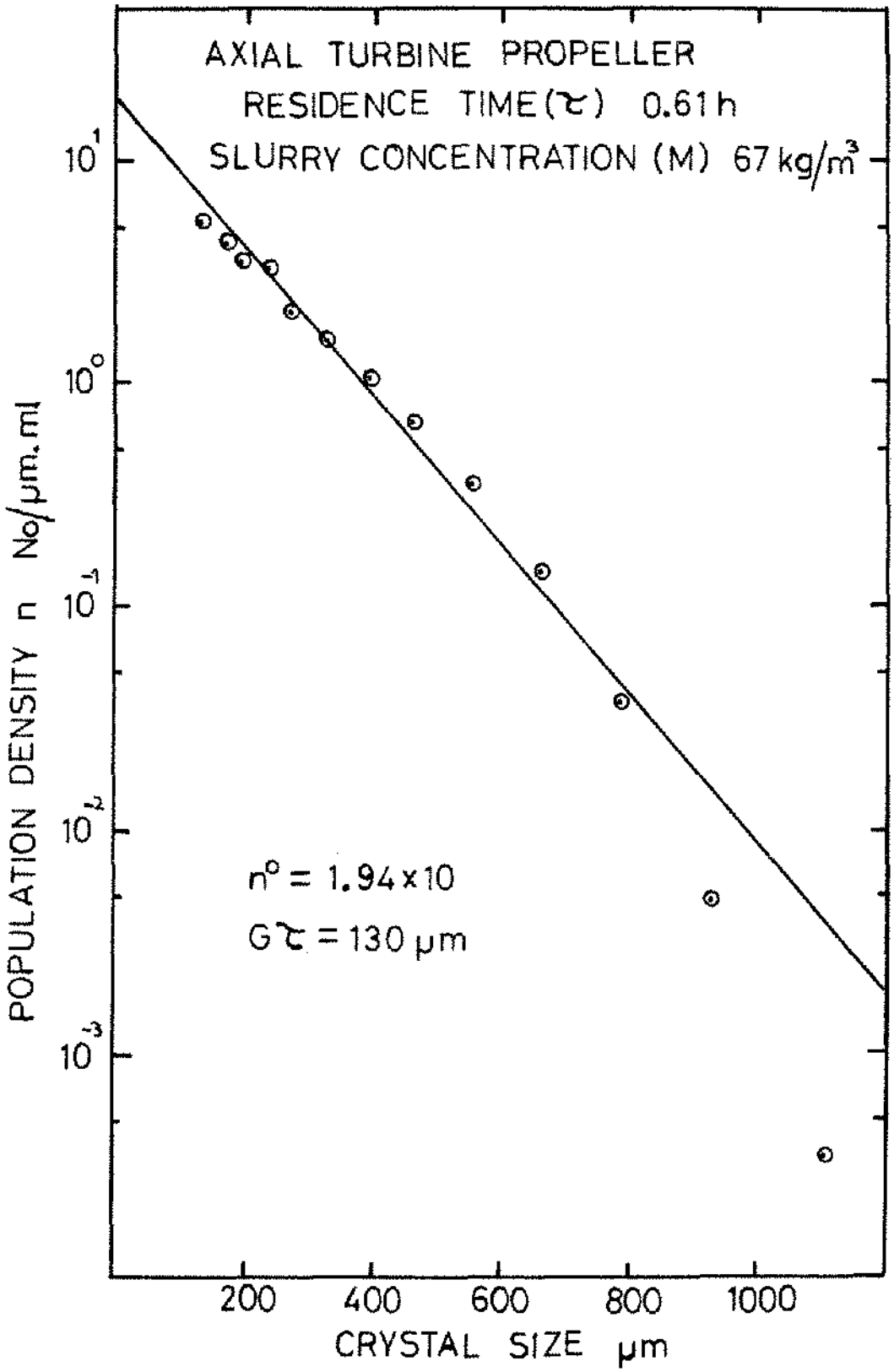

Figure 5. Steady-state population density.

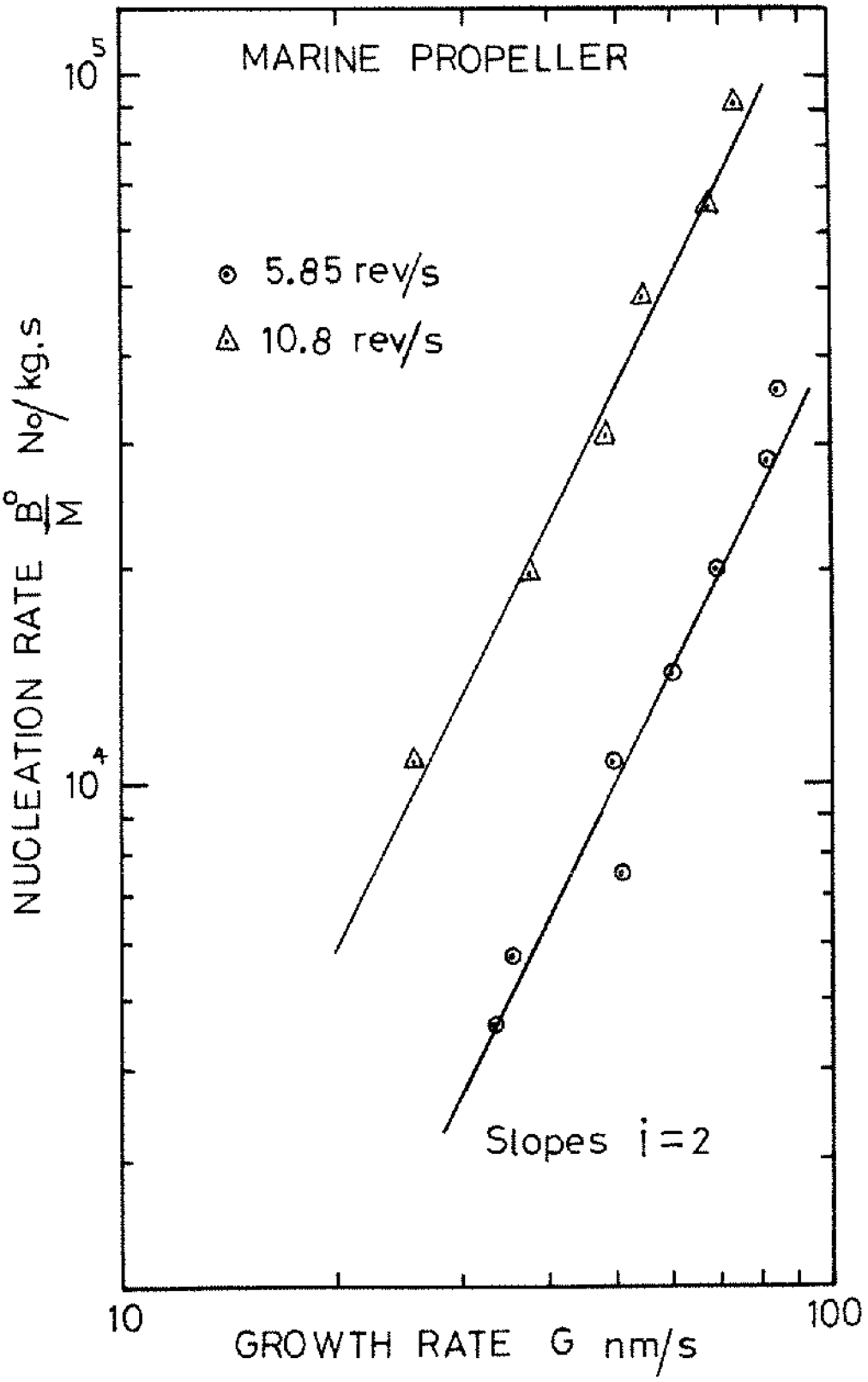

Figure 6. Nucleation rate vs. growth rate with marine propeller stirrer.

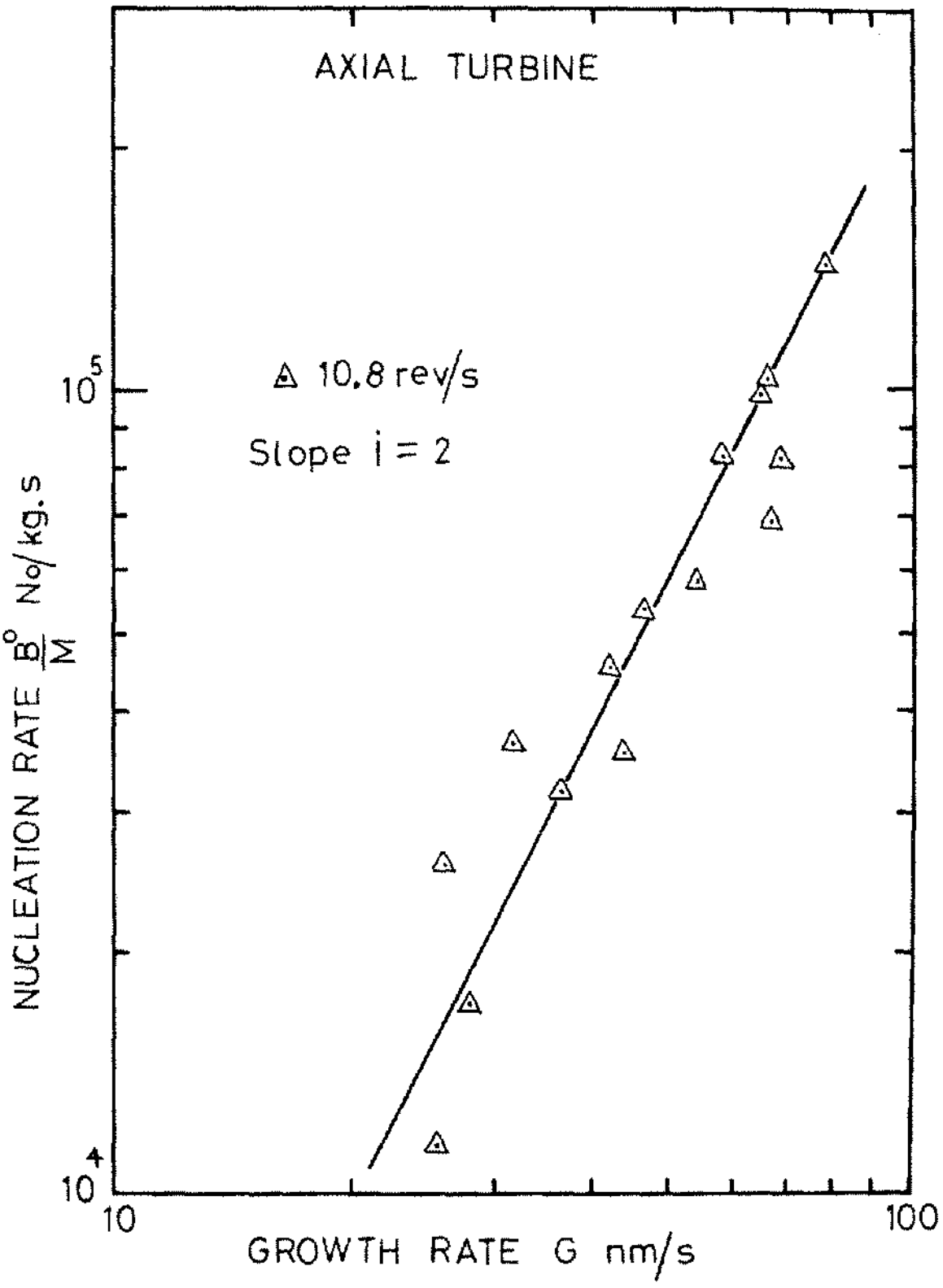

Figure 7. Nucleation rate vs. growth rate with axial turbine stirrer.

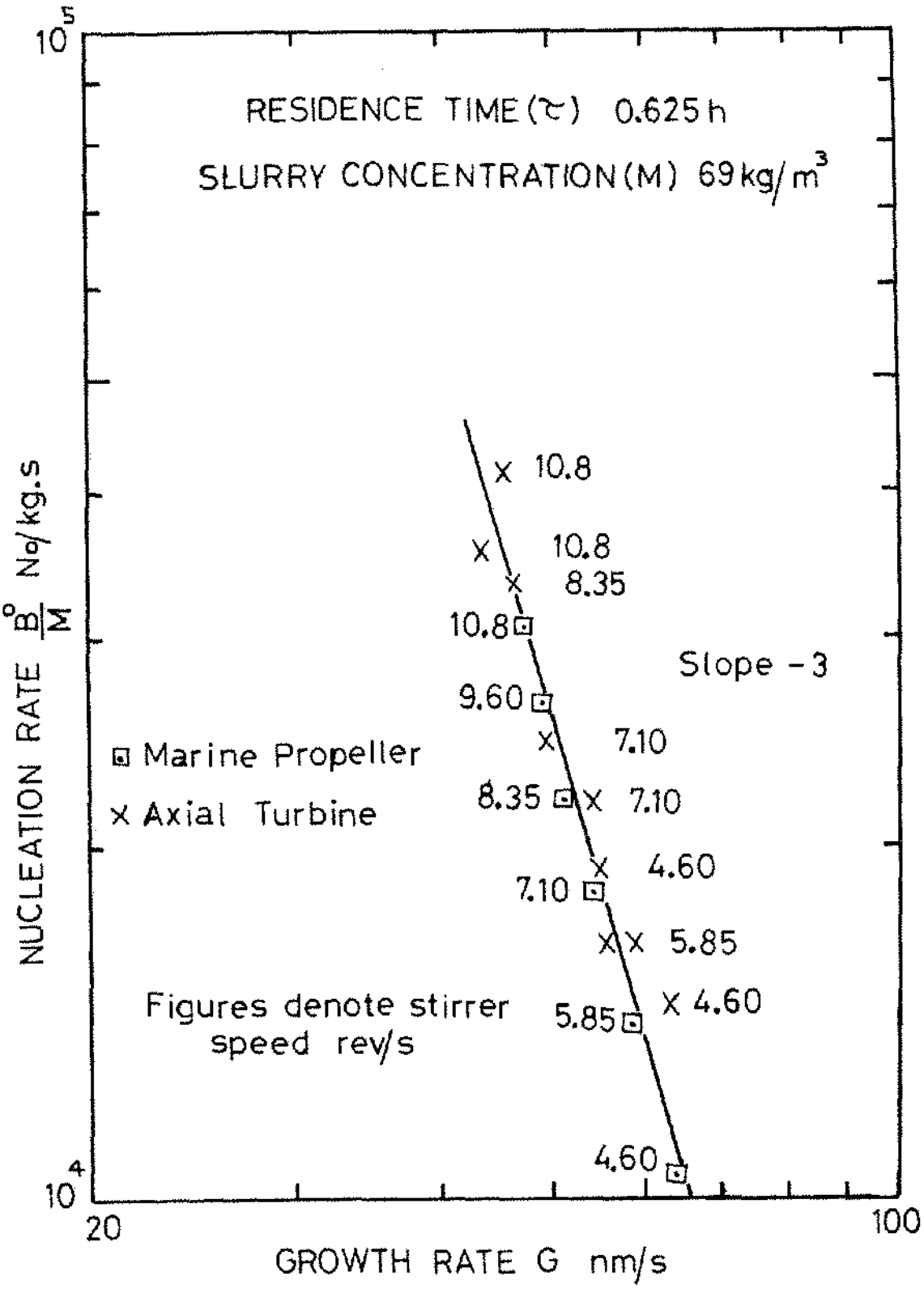

Figure 8. Variation of nucleation rate and growth rate with stirrer speed and design.

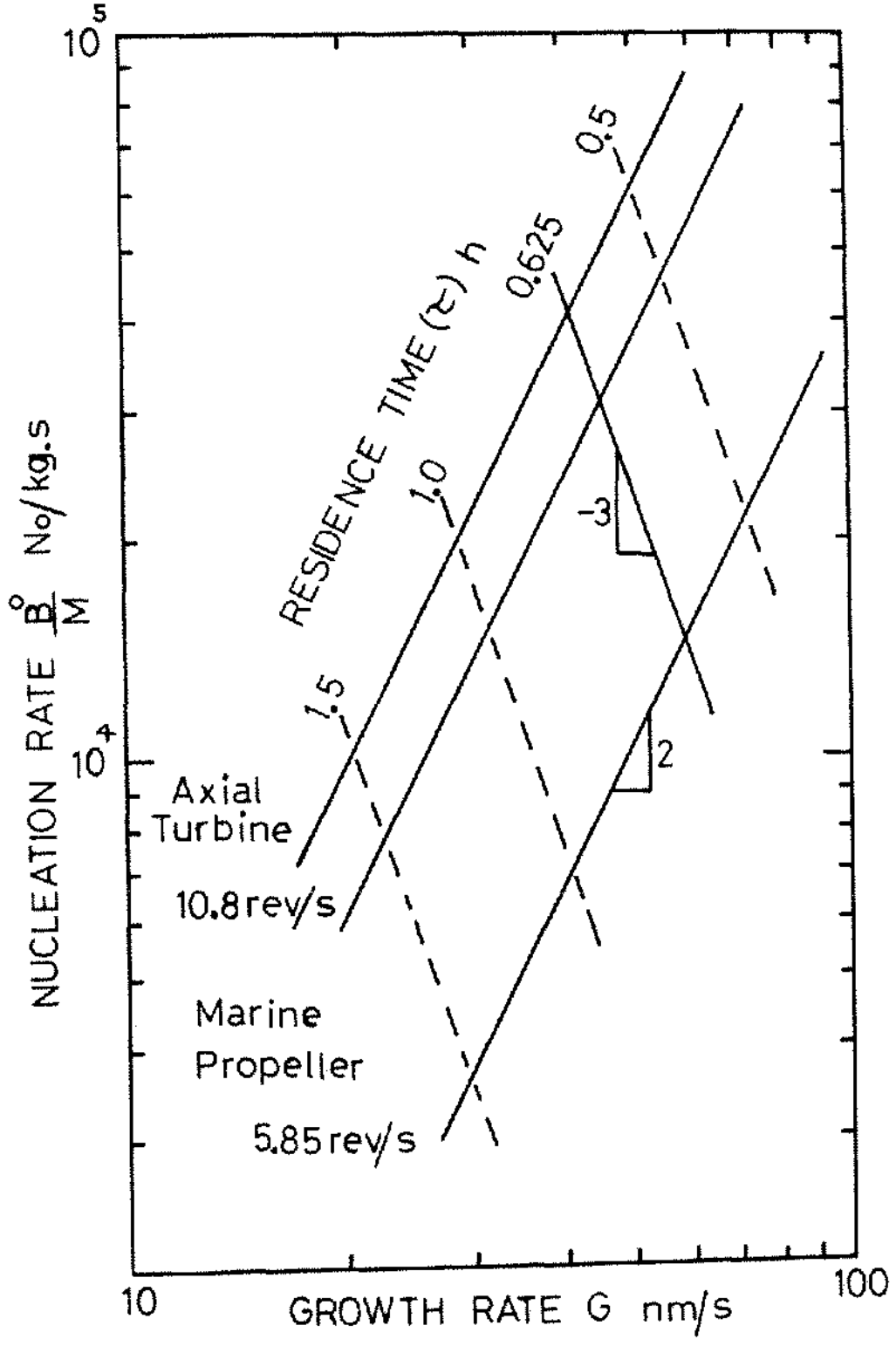

Figure 9. Variation of nucleation and growth rate with crystal residence time, stirrer speed and design.

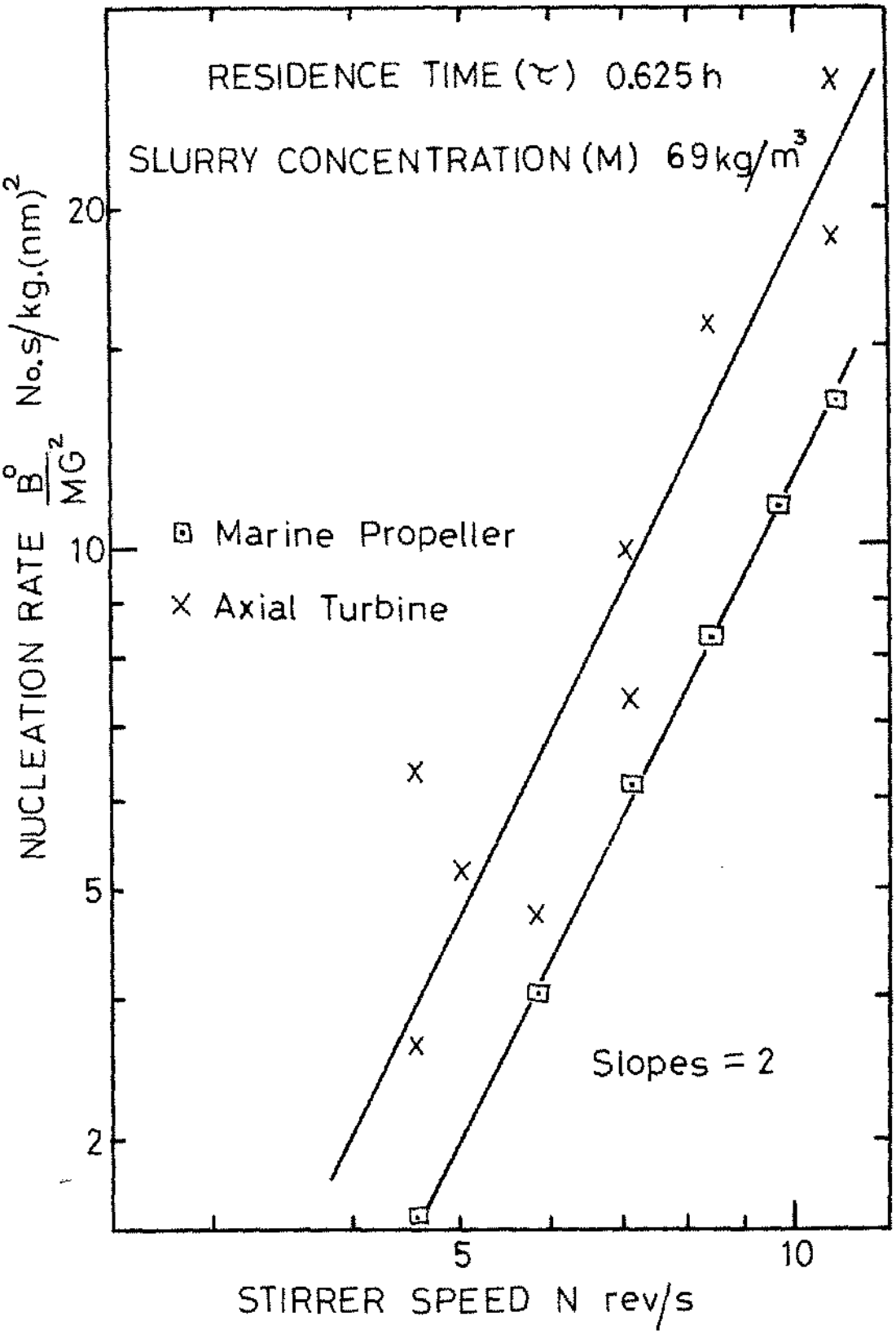

Figure 10. Nucleation rate vs. stirrer speed.

In a theoretical analysis of the effect of agitation on secondary nucleation, Nienow (13) suggests that the nucleation rate could be proportioned to N^4. It can be seen that this conclusion is not confirmed by the present study, for crystals larger than 100 μm in size.

CONCLUSIONS

It is concluded from the work reported here that:

1. Provided cubic habit salt crystals are being produced, McCabe's ΔL law of growth independent of size is obeyed over the crystal size range 100 to 1200 μm. However, this law is not obeyed when spherical or partly spherical crystals are produced.
2. The type of stirrer used in a CMSMPR crystallizer is important. The ideal design is that of a marine propeller which produces minimum crystal damage. From this, departures from 'ideal' can be evaluated.
3. Over a wide range of operating conditions, the evaporative crystallization of sodium chloride from brine can be described by a Power law model of the type $B^\circ = k_R M G^2 N^2$.

DISCUSSION

Emons:

Question. Besides nucleation and crystal growth the Ostwald-ripening and the agglomeration for crystal size, crystal shape, crystal stability are of great importance on the conditions presented. Did you make corresponding investigations? In case of a characterization of the end-product only by sieve analysis all partial-sections are obtained integral and will be falsified to some extent.

Answer. Optical examination and some crystal counts of the product crystals were made as well as sieve analysis. This examination showed that in all product samples the small crystals were either cubic in habit or fragments. The middle range of the crystal size distributions contained mainly cubes and polycrystalline material, that is cubes with smaller cubes growing out of the faces. The larger crystals were either cubes, partially rounded cubes or spheres depending on the stirrer speed and design as mentioned in the paper.

The above examination showed that the crystal shape factor varied with size, but this was not very large. In all the results reported a constant shape factor was used to calculate the number of crystals from the sieve analysis.

No investigations were made into the phenomena of Ostwald-ripening.

APPENDIX
SYMBOLS USED

Symbol		Units
B°	Nucleation rate	No/m^{3}s
C	Bulk concentration	kg/m^3
C^*	Equilibrium concentration	kg/m^3
D	Stirrer diameter	m
f_v	Volume shape factor	—
G	Linear growth rate	nm/s
k_g	Growth rate constant	
k_n	Nucleation rate constant	
k_R	Relative rate constant	
L	Crystal diameter	μm
L_m	Crystal median size—mass basis	μm
M	Mass of crystals per unit volume	kg/m^3
N	Stirrer speed	rev/s
n	Number density	No/μm ml
n°	Nuclei Population density	No/μm ml
Q	Flow rate	m^3/s
σ	Relative supersaturation $\frac{C-C^*}{C^*}$	—
S	Supersaturation	Kg/m^3
T	Temperature	°C
ρ	Crystal density	kg/m^3
τ	Mean crystal residence time	h

Exponents

m	Nucleation order in supersaturation
n	Growth order in supersaturation
i	Relative nucleation order
j	Nucleation order related to M.

ACKNOWLEDGEMENTS

The author wishes to thank Dr. D.V. Keight and the late Dr. E. Blumenthal for their helpful suggestions, also to ICI Mond Division for permission to publish this work.

REFERENCES

1. Rumford, F. and Bain, J. 1960. Trans. Instr. Chem. Eng. 38:10.
2. Randolf, A.D. and Larson, M.A. 1971. Theory of particulate processes. New York Academic Press, N.Y.
3. Larson, M.A. and Garside, J. 1973. The Chem. Eng., June, 318.
4. Bennett, R.B., et al. 1973. Chem. Eng. Prog. 69(7):86.
5. Asselbergs, C.J. and de Jong, E.J. 1972. 5th Symposium on Ind. Cryst., Paper 1-3.17, CHISA, 1972.
6. Randolf, A.D. 1970. Chem. Eng., 77(10):80.
7. Murray, J.W. and Larson, M.A. 1965. A. I. Ch. E. Journ. 11(4):728.
8. Mullin, J.W. and Garside, J. 1974. The Chem. Eng., June, 402.
9. Rosen, N. and Hulbert, M. 1969. Chem. Eng. Prog., Symp. Series 67(110):18.
10. Ramshaw, C. 1974. The Chem. Eng. July/Aug. 446.
11. Koros, W.J., et al. 1972. A. I. Ch. E., Symp. Series 68(121):67.
12. Liu, Yih-An and Botsaris, D. 1973. A. I. Ch. E. Journ. 19(3):510.
13. Nienow, A.W. 1976. Trans. Inst. Chem. Eng., 54:205.